Cellular/Molecular

Synaptotagmin 1 Is Necessary for the Ca^{2+} Dependence of Clathrin-Mediated Endocytosis

Li-Hua Yao,[1]* Yan Rao,[1]* Kelly Varga,[1] Chun-Yang Wang,[1] Peng Xiao,[2] Manfred Lindau,[3] and Liang-Wei Gong[1]

[1]Department of Biological Sciences, University of Illinois at Chicago, Chicago, Illinois 60607, [2]School of Life Science, South China Normal University, Guangzhou GD 510631, China, and [3]School of Applied and Engineering Physics, Cornell University, Ithaca, New York 14853

The role of Ca^{2+} in synaptic vesicle endocytosis remains uncertain due to the diversity in various preparations where several forms of endocytosis may contribute variably in different conditions. Although recent studies have demonstrated that Ca^{2+} is important for clathrin-mediated endocytosis (CME), the mechanistic role of Ca^{2+} in CME remains to be elucidated. By monitoring CME of single vesicles in mouse chromaffin cells with cell-attached capacitance measurements that offer millisecond time resolution, we demonstrate that the dynamics of vesicle fission during CME is Ca^{2+} dependent but becomes Ca^{2+} independent in synaptotagmin 1 (Syt1) knock-out cells. Our results thus suggest that Syt1 is necessary for the Ca^{2+} dependence of CME.

Introduction

Neurotransmitter release is mediated by exocytosis of synaptic vesicles, and subsequent endocytosis is essential for supporting rapid and repeated rounds of release (Stevens, 2003). Although the roles of Ca^{2+} in exocytosis are well established (Zucker and Regehr, 2002; Neher and Sakaba, 2008), its role in synaptic vesicle endocytosis remains uncertain (Ceccarelli and Hurlbut, 1980; Ramaswami et al., 1994; von Gersdorff and Matthews, 1994; Cousin and Robinson, 1998; Gad et al., 1998; Marks and McMahon, 1998; Beutner et al., 2001; Neves et al., 2001; Sankaranarayanan and Ryan, 2001; Wu et al., 2005), largely because the results are diverse among various preparations where several forms of endocytosis may contribute variably in different conditions (Wu et al., 2007). It has been recently demonstrated that Ca^{2+} is critical in clathrin-mediated endocytosis (CME), the slow form of endocytosis, in the calyx of Held (Hosoi et al., 2009; Wu et al., 2009). However, it remains to be shown how Ca^{2+} regulates the process of CME and which molecules determine the Ca^{2+} dependence of CME. In the present study, CME of single vesicles was monitored using cell-attached capacitance measurements, in which a sinusoidal voltage was superimposed to the holding potential and a two-phase lock-in amplifier was used to analyze the current output signal. When the phase of the lock-in amplifier was properly adjusted, the two outputs of the amplifier directly provided the changes of membrane conductance in one channel and the changes of membrane capacitance in the other channel (Neher and Marty, 1982; Debus and Lindau, 2000). When the tubular membrane neck that connects the endocytic vesicle to the plasma membrane before vesicle pinch-off has a low conductance, the vesicle capacitance (Cv) is not fully charged and the values in the capacitance trace are reduced while a transient increase in the conductance trace appears. As for exocytotic fusion pores (Debus and Lindau, 2000), the analysis of these changes can be used to estimate the dynamic behavior of endocytic fission-pore conductance (Gp) (Rosenboom and Lindau, 1994; Dernick et al., 2003; MacDonald et al., 2005; Zhao et al., 2010). Our results demonstrate that the dynamics of vesicle fission during CME is Ca^{2+} dependent but becomes Ca^{2+} independent in synaptotagmin 1 (Syt1) knock-out (KO) cells, indicating that Syt1 is required for the Ca^{2+} dependence of CME.

Materials and Methods

Chromaffin cell culture. Adrenal glands of newborn pups of either sex (postnatal day 0) from wild-type (WT) or Syt1 heterozygous (HT) mouse matings were isolated in accordance with the guidelines of the National Institutes of Health, as approved by the Animal Care and Use Committee of the University of Illinois at Chicago. Tails were kept for genotyping for newborn pups from Syt1 HT matings, and electrophysiological recordings on chromaffin cell cultures from littermate WT and Syt1 KO mice were compared. WT chromaffin cells were typically from WT matings, except that WT chromaffin cells for data presented in Figure 3 were from Syt1 HT matings.

Mouse chromaffin cells were prepared and cultured as previously described (Gong et al., 2005). The following solutions were prepared and sterile filtered (0.22 μm): papain solution, 250 ml of DMEM (Invitrogen) was supplemented with 50 mg of L-cysteine/1 mM $CaCl_2$/0.5 mM EDTA/20–25 U/ml papain (Worthington), and equilibrated with 5% CO_2; inactivating solution, 225 ml of DMEM was supplemented with 25 ml of heat-inactivated FCS/625 mg of albumin/625 mg of trypsin inhibitor (Sigma); enriched DMEM, 500 ml of DMEM was supplemented with 5 ml of penicillin/streptomycin (Invitrogen)/5 ml of insulin-transferrin-selenium-X (Invitrogen); and Locke's solution, 154 mM NaCl/5.6 mM KCl/3.6 mM $NaHCO_3$/10 mM glucose, pH 7.3 with NaOH. Adrenal glands were dissected from newborn mice and placed in filtered Locke's solution. Contaminating tissue was removed by dissection. The glands

Received July 11, 2011; revised Jan. 23, 2012; accepted Jan. 27, 2012.

Author contributions: L.-H.Y., Y.R., and L.-W.G. designed research; L.-H.Y., Y.R., K.V., C.-Y.W., P.X., M.L., and L.-W.G. performed research; L.-H.Y., Y.R., P.X., M.L., and L.-W.G. analyzed data; L.-H.Y., Y.R., M.L., and L.-W.G. wrote the paper.

This work was supported by the University of Illinois at Chicago startup fund, Brain Research Foundation Grant BRF SF 2010-06, and National Science Foundation Award 1145581 to L.-W.G. We thank Dr. J. Morgan (University of Texas at Austin) for critical reading of this manuscript.

*L.-H.Y. and Y.R. contributed equally to this work.

Correspondence should be addressed to Liang-Wei Gong, Department of Biological Sciences, University of Illinois at Chicago, 840 West Taylor Street, Chicago, IL 60607. E-mail: lwgong@uic.edu.

DOI:10.1523/JNEUROSCI.3540-11.2012

 0270-6474/12/323778-08$15.00/0

were incubated in 1 ml of papain solution at 37°C for 40 min and inactivated by addition of 0.75 ml of the inactivating solution for another 10 min. The medium was carefully replaced with 0.2 ml of enriched DMEM, and the glands were triturated gently through a 200 μl pipette tip. Seventy microliters of the cell aliquots were plated on 12 mm coverslips coated with poly-D-lysine (Sigma), and cells were allowed to attach before supplemented with 2 ml of enriched medium. The cells were incubated at 37°C in 5% CO_2 and used within 4 d.

Solutions. The bath solution contained 140 mM NaCl, 5 mM KCl, 2 mM $CaCl_2$, 1 mM $MgCl_2$, 10 mM HEPES-NaOH, and 10 mM glucose; the pH was adjusted to 7.3 with NaOH, and the osmolarity was ~310 mmol kg^{-1}. The solution in the cell-attached pipette contained 50 mM NaCl, 100 mM TEACl, 5 mM KCl, 2 mM $CaCl_2$, 1 mM $MgCl_2$, and 10 mM HEPES-NaOH; the pH was adjusted to 7.3 with NaOH, and the osmolarity was adjusted to 290 mmol kg^{-1}. The solution in the whole-cell pipette for the double (cell-attached/whole-cell) patch approach contained 20 mM CsCl, 100 mM KCl, 20 TEACl, 1 mM $MgCl_2$, 10 mM HEPES, 2 mM MgATP, and 0.3 Na_3GTP; the pH was adjusted to 7.3 with KOH, and the osmolarity was adjusted to 290 mmol kg^{-1}. Basal $[Ca^{2+}]_i$ in the whole-cell pipette solutions was buffered by 1.1 mM $CaCl_2$ and 2 mM EGTA to give a final free $[Ca^{2+}]_i$ of ~150 nM.

Cell-attached capacitance recordings. Changes in membrane capacitance and conductance were recorded by the cell-attached capacitance technique of patch-clamp (Debus and Lindau, 2000; Dernick et al., 2005). Patch pipettes were pulled in four stages with a programmable P-97 puller (Sutter Instruments) and coated with a sticky wax (Kerr). Pipettes were fire polished and had a typical resistance of ~2 MΩ in the bath solution. For cell-attached capacitance measurements, an EPC-7 plus patch-clamp amplifier (HEKA Elektronik) was used. Command voltage was applied to the bath solution. Changes of patch admittance were measured, as described previously (Debus and Lindau, 2000), with a SR830 lock-in amplifier (Stanford Research Systems) using a sine-wave amplitude of 50 mV (root mean square) at a frequency of 20 kHz. The output filter of the lock-in amplifier was set to a 1 ms time constant, 24 db. The phase of the lock-in amplifier was set such that transient capacitance changes produced by gentle suction pulses appeared only in the patch capacitance (Im) trace, with no projection into the patch conductance (Re) trace (Debus and Lindau, 2000). Because the phase may change during the recording, the phase for sections with endocytic events of interest was readjusted such that the baseline of the Re trace was at the same level before and after completion of the capacitance step.

All endocytic events were recorded by the cell-attached patch configuration unless mentioned otherwise. Capacitance steps and fission-pore durations were reliably detected for step sizes >0.2 fF, and smaller steps were not included in the analysis. The number of endocytic events per patch detected in the cell-attached recordings was counted as the total number of downward capacitance steps within the first 5 min of recordings.

Double (cell-attached/whole-cell) patch recordings. The endocytic events were also recorded by the double (cell-attached/whole-cell) patch configuration in some experiments. In this double-patch configuration, the cells held at −65 mV were stimulated by a train of 100 ms depolarization to 0 mV at 0.2 Hz through the whole-cell pipette to induce endocytosis of single vesicles that were recorded by the other cell-attached patch pipette. The number of endocytic events recorded per patch in this double (cell-attached/whole-cell) patch configuration was counted as the total number of downward capacitance steps >0.2 fF within 5 min of the first depolarization.

Fission-pore analysis. Fission-pore closures of endocytic events were analyzed in the same way as exocytotic fusion-pore openings as described previously (Debus and Lindau, 2000; Dernick et al., 2005; Gong et al., 2007). During fission-pore closure of endocytic events in which a transient increase in the Re signal was associated with a decline in the Im step, the Cv was determined as the total change in the Im trace for a particular event and the Gp was calculated using the formula $Gp = \frac{\omega C\nu}{\sqrt{\left(\frac{\omega C\nu}{Im}\right) - 1}}$ (Breckenridge and Almers, 1987). The fission-pore duration was defined as the time interval from the first point where Gp decreased below 2 nS and the final drop in Gp to zero. This final drop reflects the step response of the low-pass filter setting of the lock-in amplifier (1 ms, 24 dB). At this setting, 90% of the final value is reached within ~7 ms, so the last point of the fission-pore was taken as the time at 7–10 ms before the final drop to zero in the Gp trace. The Gp was taken as the average Gp value during the fission-pore duration time interval. Analysis of fission-pore kinetics was restricted to fission pores with durations >15 ms, because shorter events were distorted by the lock-in amplifier low-pass filter (set to 1 ms, 24 dB).

Amperometry. Conventional carbon fiber amperometry for catecholamine detection used 5 μm carbon fibers (ALA Scientific Instruments) as described previously (Gong et al., 2005, 2007). The freshly cut tip of the carbon fiber electrode was positioned closely against the cell surface to minimize the diffusion distance from release sites. The amperometric current, generated by catecholamine oxidation at the exposed tip of the carbon fiber electrode, was measured using an EPC-7 plus amplifier, operated in the voltage-clamp mode at a holding potential of +700 mV. Amperometric signals were low-pass filtered at 1 kHz and digitized at 4 kHz. Similar to the stimulation pattern in double-patch configuration, secretion was induced by a train of 100 ms depolarization to 0 mV at 0.2 Hz through a whole-cell patch pipette. Amperometric recordings were collected and then analyzed with a customized macro for IGOR software (WaveMetrics) to extract spike information according to the criteria of Chow et al. (1992). The number of amperometric spikes was counted as the total number of spikes with an amplitude >10 pA within 120 s of the first depolarization.

Reagents. Anti-clathrin heavy chain antibody (X22) was obtained from Affinity BioReagents. The KR-peptide, a Syt1 C2B domain-derived peptide with the sequence of KRLKKKKTTIKK, was used to block the interaction of Syt1 and AP-2 (the clathrin adaptor protein complex) (Grass et al., 2004). The control experiments were performed using the scrambled version of the KR-peptide (Scr-peptide, KKKRTLTKKKKI) and the mutant version of the KR-peptide (AA-peptide, KRLKKAATTIKK) with two of the conserved lysines (KK) replaced by alanines (AA), which displays no interaction with AP-2, as shown by a previous study (Kastning et al., 2007). These three peptides were synthesized by Biomatik and NeoBioscience. The intracellular application of anti-clathrin heavy chain antibody, KR-peptide, Scr-peptide, or AA-peptide was through a whole-cell patch pipette for at least 15 min in the double (cell-attached/whole-cell) patch configuration while endocytosis of single vesicles was recorded by the other cell-attached patch pipette.

Statistical analysis. All the experiments were performed at room temperature. Data are expressed as mean ± SEM, and Newman one-way ANOVA tests were used for statistical analysis. Because typically one or two analyzable endocytic events can be obtained from each individual cell, every endocytic event was treated as statistically independent and the number of events was used for statistical testing of the fission-pore kinetics.

Results

Figure 1*A* shows a recording with both upward and downward capacitance steps. In this recording, the upward capacitance steps, which are associated with exocytosis as reported previously (Gong et al., 2003, 2007), occurred at earlier times than the downward capacitance steps associated with endocytosis (Fig. 1*A*). The plot of endocytic events, as a function of time, shows that the frequency of endocytic events increased after the first depolarization (Fig. 1*B*), suggesting that the stimulation effectively increased the rate of endocytotic events. The diameter of individual vesicles associated with endocytosis was calculated assuming a specific capacitance of 9 fF/μm^2 (Albillos et al., 1997; Gong et al., 2003) and spherical geometry. The resulting frequency distribution of vesicle diameters for these endocytic events did not show evidence of a multimodal distribution (Fig. 1*C*), suggesting that the downward capacitance steps reflect a single type of endocytic events. Figure 1*D* exemplifies a cell-attached recording with Re (top) and Im (bottom) in a control chromaffin cell. This trace displays five downward capacitance

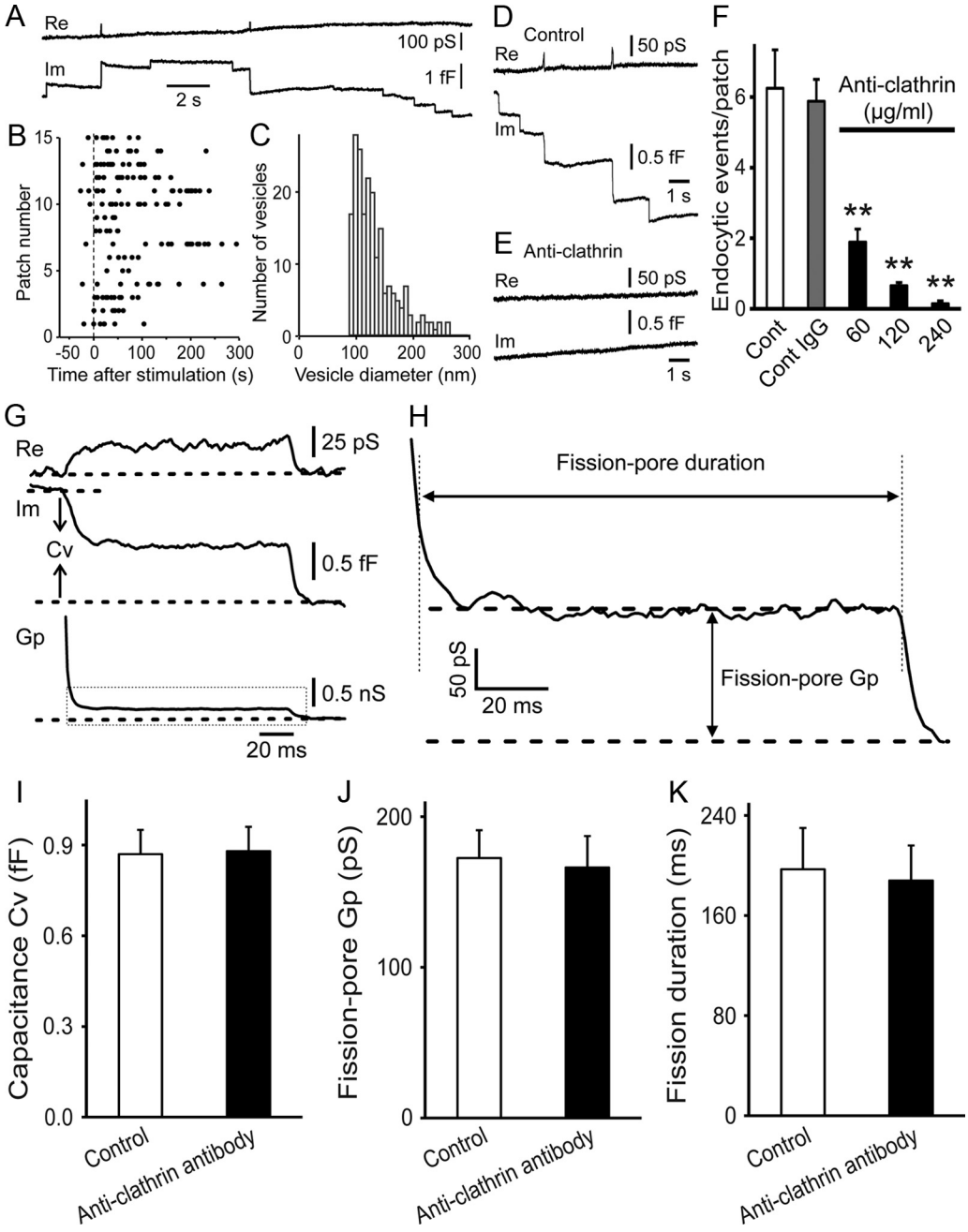

Figure 1. CME of single vesicles and the fission-pore analysis. ***A***, Simultaneous recordings of Re and Im by a cell-attached patch pipette in the double (cell-attached/whole-cell) patch configuration showed upward capacitance steps associated with exocytosis and downward capacitance steps associated with endocytosis. ***B***, The occurrence of individual endocytic events as a function of time for each of 15 patches with at least six endocytic events. Each dot represents an individual endocytic event and the vertical dotted line indicates the onset of stimulation. ***C***, Distribution of vesicle diameters derived from endocytic capacitance step sizes. The mean vesicle diameter is 122 ± 2.7 nm ($n = 238$ events). ***D***, ***E***, Downward steps in Im associated with single vesicle endocytosis in a control cell (***D***) were largely abolished in a cell treated with 240 μM anti-clathrin heavy chain antibody (***E***). ***F***, Statistical analysis demonstrating that applications of anti-clathrin heavy chain antibody through the whole-cell patch pipette significantly decreased the number of endocytic events recorded within 5 min by the cell-attached patch pipette (Control: $n = 48$ patches; 240 μg/ml Control IgG: $n = 40$ patches, $p > 0.05$; 60 μg/ml anti-clathrin antibody: $n = 75$ patches, $p < 0.01$; 120 μg/ml anti-clathrin antibody: $n = 28$ patches, $p < 0.01$; 240 μg/ml anti-clathrin antibody: $n = 30$ patches, $p < 0.01$). **$p < 0.01$. ***G***, Analysis of an individual fission-pore closure event. The traces from top to bottom show the time course of: Re, Im, and fission-pore conductance Gp. Cv is indicated in Im trace. ***H***, The dotted box in ***G*** is shown on an expanded scale. The fission-pore kinetics were characterized by the fission-pore conductance Gp, and the duration as indicated. ***I–K***, Application of anti-clathrin antibody at 60 μg/ml through a whole-cell patch pipette did not alter the mean Cv of the endocytic vesicles (Control: 0.87 ± 0.08 fF, $n =$ 47 events; Anti-clathrin antibody: 0.88 ± 0.08 fF, $n = 45$ events, $p > 0.05$) (***I***), the fission-pore conductance Gp (Control: 173 ± 18 pS; Anti-clathrin antibody: 166 ± 21 pS, $p > 0.05$) (***J***), and the fission-pore duration (Control: 197 ± 33 ms; Anti-clathrin antibody: 188 ± 28 ms, $p > 0.05$) (***K***).

steps, indicating sequential endocytosis of five individual vesicles. When an anti-clathrin heavy chain antibody was delivered into the cells through the whole-cell pipette in double (cell-attached/whole-cell) patch configuration, the number of endocytic events detected by the cell-attached pipette was significantly decreased in a concentration-dependent manner ($p < 0.01$) while control IgG had no significant effect (Fig. 1*E*,*F*), demonstrating that these endocytic events represent CME. For a subset of individual endocytic event, the decrease in Im was associated with a detectable transient change in the Re trace, reflecting detection of a

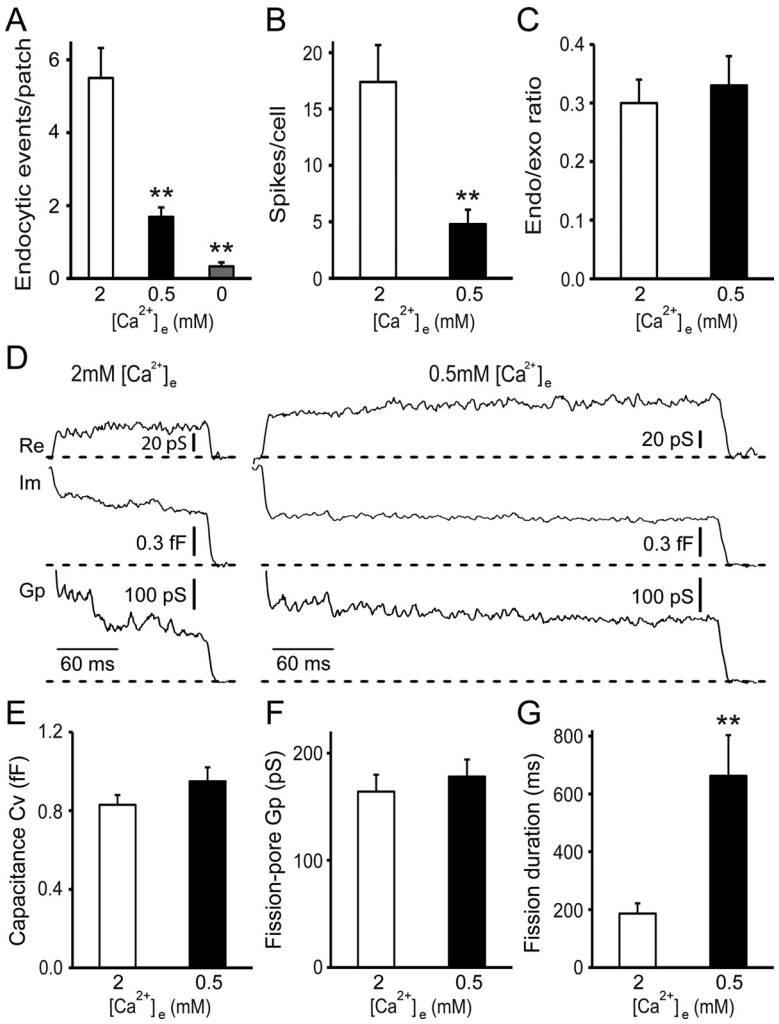

Figure 2. Dependence of endocytic event properties on $[Ca^{2+}]_e$. ***A***, The number of endocytic events within 5 min of cell-attached recordings was reduced by ~70% at 0.5 mM $[Ca^{2+}]_e$ ($n = 102$ patches) ($p < 0.01$) and by ~95% at zero $[Ca^{2+}]_e$ ($n = 46$ patches) ($p < 0.01$), compared to 2 mM $[Ca^{2+}]_e$ ($n = 95$ patches). Zero $[Ca^{2+}]_e$ was achieved through a combination of removal of Ca^{2+} and addition of 5 mM EGTA. ***B***, The number of amperometric spikes at 0.5 mM $[Ca^{2+}]_e$ ($n = 18$ cells) was reduced compared to 2 mM $[Ca^{2+}]_e$ ($n = 18$ cells) ($p < 0.01$). The experiments in ***A*** and ***B*** were performed on different cells from the same preparations. ***C***, The endocytosis/exocytosis ratio did not differ statistically between 2 and 0.5 mM $[Ca^{2+}]_e$ ($p > 0.05$). ***D***, Representative fission-pore events at 2 mM (left) and 0.5 mM $[Ca^{2+}]_e$ (right) in the cell-attached patch configuration. ***E***, The mean capacitance step size of endocytic vesicles was indistinguishable between these two groups (2 mM $[Ca^{2+}]_e$: $n = 43$ events; 0.5 mM $[Ca^{2+}]_e$: $n = 42$ events) ($p > 0.05$). ***F***, The fission-pore Gp was independent of $[Ca^{2+}]_e$ ($p > 0.05$). ***G***, The fission-pore duration was significantly increased ($p < 0.01$) at 0.5 mM $[Ca^{2+}]_e$. $^{**}p < 0.01$.

narrow fission-pore (Fig. 1*G*), which was characterized by the fission-pore Gp and duration (Fig. 1*H*). We then examined the fission-pore kinetics of endocytic events in cells treated with 60 μg/ml anti-clathrin heavy chain antibody, which inhibited the number of endocytic events by ~65% (Fig. 1*F*), because treatments with this antibody at concentrations of 120 or 240 μg/ml reduced the occurrence of endocytic events to such a low level that a statistical analysis was impossible. Our results showed that cells pretreated with 60 μg/ml antibody displayed no changes in the capacitance step size of the endocytic vesicles (Fig. 1*I*), the fission-pore Gp (Fig. 1*J*), or the fission-pore duration (Fig. 1*K*). It has been shown by electron microscopy that AP-2 and associated endocytic accessory proteins assemble into coated membrane subdomains that lack any significant curvature in the absence of clathrin, demonstrating that clathrin is important for invagination during CME (Nossal, 2001; Hinrichsen et al., 2006). Our results thus indicate that the fission-pore kinetics cannot be affected by defect in endocytic invagination.

The endocytic events observed in the cell-attached recordings are Ca^{2+} dependent and triggered by Ca^{2+} influx into the cell during patching, because removal of external Ca^{2+} substantially reduced the occurrence of these events ($p < 0.01$) (Fig. 2*A*). The number of endocytic events was decreased by ~70% at 0.5 mM $[Ca^{2+}]_e$ compared to 2 mM $[Ca^{2+}]_e$ ($p < 0.01$) (Fig. 2*A*). Meanwhile, exocytosis, as measured by carbon fiber amperometry, was also inhibited to a similar extent at 0.5 mM $[Ca^{2+}]_e$ ($p < 0.01$) (Fig. 2*B*). As a result, the endocytosis/exocytosis ratio was indistinguishable at 2 and 0.5 mM $[Ca^{2+}]_e$ ($p > 0.05$) (Fig. 2*C*), suggesting that the inhibition in endocytosis at lower $[Ca^{2+}]_e$ may be a consequence of the reduction in exocytosis. The capacitance step size (Fig. 2*D*,*E*) and the fission-pore Gp (Fig. 2*D*,*F*) of these endocytic events were not statistically different in these two groups ($p > 0.05$). However, the fission-pore duration was prolonged by ~250% at 0.5 mM $[Ca^{2+}]_e$, compared to 2 mM $[Ca^{2+}]_e$ ($p < 0.01$) (Fig. 2*D*,*G*), indicating a direct role of Ca^{2+} in vesicle fission during CME.

Given the Ca^{2+} binding capability of Syt1 and its putative role as the Ca^{2+} sensor in exocytosis (Chapman, 2008; Pang and Südhof, 2010), we tested whether Syt1, the predominant synaptotagmin isoform in chromaffin cells (Marquèze et al., 1995), may be responsible for the Ca^{2+} sensitivity of fission-pore dynamics during CME by examining the fission-pore kinetics of endocytic events in Syt1 KO cells (Fig. 3*A*). There was a significant decrease in the number of endocytic events in KO cells compared to WT cells ($p < 0.01$) (Fig. 3*B*). Although exocytosis, as measured by carbon fiber amperometry, was also inhibited ($p < 0.01$) (Fig. 3*C*), the endocytosis/exocytosis ratio was decreased in KO cells ($p < 0.01$) (Fig. 3*D*), pointing to a direct role of Syt1 in CME beyond exocytosis. Both the capacitance step size of endocytic vesicles (Fig. 3*A*,*E*) and the fission-pore Gp (Fig. 3*A*,*F*) were indistinguishable between WT and KO cells ($p > 0.05$). However, the fission-pore duration was increased by ~150% in KO cells compared to WT cells ($p < 0.01$) (Fig. 3*A*,*G*). Comparison of the fission-pore durations at 2, 1, and 0.5 mM $[Ca^{2+}]_e$ between WT and KO cells revealed that the Ca^{2+} dependence of the fission-pore duration observed in WT cells was abolished in Syt1 KO cells (Fig. 3*H*), indicating that the Ca^{2+} dependence of fission dynamics during CME requires Syt1.

Because Syt1 interacts with the endocytic adaptor AP-2 (Zhang et al., 1994; Chapman et al., 1998; Haucke and De Camilli, 1999; Grass et al., 2004), we tested whether the alterations in the endocytosis/exocytosis ratio and in the fission-pore kinetics

in Syt1 KO cells are mediated by this interaction. Disruption of Syt1–AP-2 binding was fashioned using a peptide derived from the Syt1 C2B domain (KR-peptide with the sequence of KRLKKKKTTIKK), which is essential for the Syt1–AP-2 interaction (Grass et al., 2004). When the KR-peptide was delivered into the cells through the whole-cell patch pipette in the double (cell-attached/whole-cell) patch configuration, the number of endocytic events recorded at 2 mM $[Ca^{2+}]_e$ was inhibited in a concentration-dependent manner ($p < 0.01$) (Fig. 4*A*). On the other hand, carbon fiber amperometry experiments showed that this KR-peptide had no effects on exocytosis (Fig. 4*B*), indicating a specific role of the Syt1–AP-2 interaction in endocytosis. As a consequence, the endocytosis/exocytosis ratio was reduced in cells treated with this KR-peptide ($p < 0.01$) (Fig. 4*C*). Both a scrambled version of the KR-peptide (Scr-peptide) and a mutant version of the KR-peptide, which displayed no interaction with AP-2 (Kastning et al., 2007) (AA-peptide), had no significant effects on endocytosis (Fig. 4*A*), exocytosis (Fig. 4*B*), or the endocytosis/exocytosis ratio (Fig. 4*C*) ($p > 0.05$), thus supporting the specificity of the KR-peptide. These results thus suggest that the reduction in the endocytosis/exocytosis ratio in Syt1 KO cells (Fig. 3*D*) may be likely due to the disrupted Syt1–AP-2 interaction.

To determine whether the KR-peptide changes the fission-pore kinetics, the endocytic events measured at 25 μM peptide concentration were analyzed because too few endocytic events could be obtained in cells dialyzed with this peptide at 100 μM (Fig. 4*A*). The capacitance step size of the endocytic vesicles (Fig. 4*D*) and the fission-pore Gp (Fig. 4*E*) were indistinguishable between control cells and cells treated with the KR-peptide ($p > 0.05$). Notably, and in contrast to Syt1 KO cells, the KR-peptide had no effect on the fission-pore duration at 2 mM $[Ca^{2+}]_e$ ($p > 0.05$) (Fig. 4*F*). Moreover, in both control cells and cells treated with 25 μM KR-peptide, the fission-pore duration was increased in a similar fashion by a factor of ~2 when lowering $[Ca^{2+}]_e$ from 2 to 1 mM (Fig. 4*F*). Meanwhile, treatments with the Scr-peptide and the AA-peptide did not alter the capacitance step size of the endocytic vesicle (Fig. 4*D*), the fission-pore Gp (Fig. 4*E*), or the fission-pore duration (Fig. 4*F*) at both 2 and 1 mM $[Ca^{2+}]_e$ ($p > 0.05$). These results indicate that, with KR-peptide at a concentration that produces partial inhibitions, the remaining CME events were still mediated by Syt1 while a higher peptide concentration resulted in full inhibitions. In contrast, inhibition was incomplete in Syt1 KO but the remaining events showed Ca^{2+}-independent fission-pore dynamics. The most likely explanation for these results is that, in Syt1 KO cells, CME is mediated by other synaptotagmin isoforms with presumably no or low Ca^{2+} affinity than Syt1.

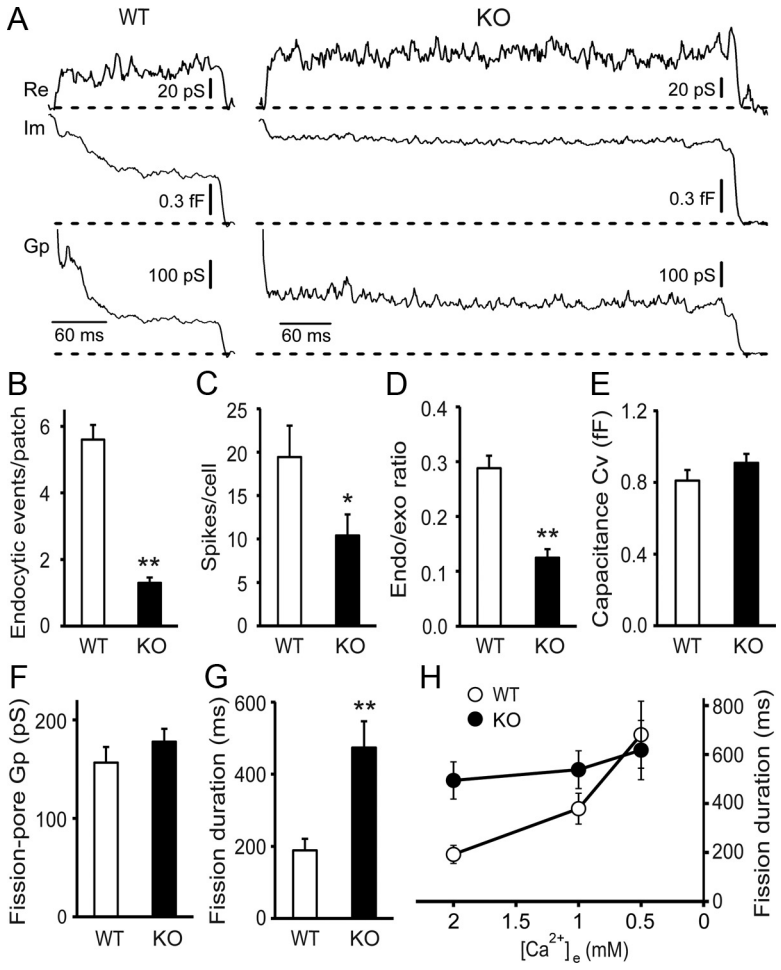

Figure 3. The fission-pore duration is prolonged and its Ca^{2+} dependence is abolished in Syt1 KO cells. ***A***, Representative fission-pore events at 2 mM $[Ca^{2+}]_e$ in WT (left) and Syt1 KO cells (right) recorded in the cell-attached patch configuration. ***B***, The number of endocytic events within 5 min of recordings was reduced in Syt1 KO cells ($n = 281$ patches) compared to WT cells ($n = 89$ patches) ($p < 0.01$). ***C***, The number of amperometric spikes was decreased in Syt1 KO cells (WT: $n = 21$ cells; KO: $n = 21$ cells) ($p < 0.05$). The experiments in ***B*** and ***C*** were performed on different cells from the same preparations. ***D***, The endocytosis/exocytosis ratio was also reduced in Syt1 KO cells ($p < 0.01$). ***E–G***, In Syt1 KO cells, Cv of the endocytic vesicles (***E***) and the fission-pore conductance Gp (***F***) were indistinguishable between WT ($n = 52$ events) and KO cells ($n = 43$ events) ($p > 0.05$), but the fission-pore duration was significantly increased ($p < 0.01$) (***G***). ***H***, The fission-pore duration was significantly dependent on $[Ca^{2+}]_e$ in WT cells (2 mM: $n = 44$ events, 1 mM: $n = 49$ events, $p < 0.01$; 0.5 mM: $n = 46$ events, $p < 0.01$) but not in Syt1 KO cells (2 mM: $n = 42$ events, 1 mM: $n = 50$ events, $p > 0.05$; 0.5 mM: $n = 39$ events, $p > 0.05$). *$p < 0.05$; **$p < 0.01$.

Discussion

In the present study, we monitored CME of single vesicles by two different configurations: cell-attached patch configuration, where endocytic events may be spontaneous and/or triggered by mechanical stimulation during patching, and the double (cell-attached/whole-cell) patch configuration, where endocytic events are stimulated by a train of depolarizations applied through the whole-cell patch pipette. The number of exocytotic events, which coexist with these endocytic events, as shown in Figure 1*A*, was increased in the double (cell-attached/whole-cell) patch configuration compared to cell-attached patch configuration (data not shown), indicating that the depolarizations were effective in stimulating exocytosis. Our results showed that the frequency of endocytic events was also increased after stimulation (Fig. 1*B*). It may, therefore, be expected that the number of endocytic events recorded in the double-patch configuration would be higher than that in the cell-attached patch configuration. However, contrary to this expectation, our results showed

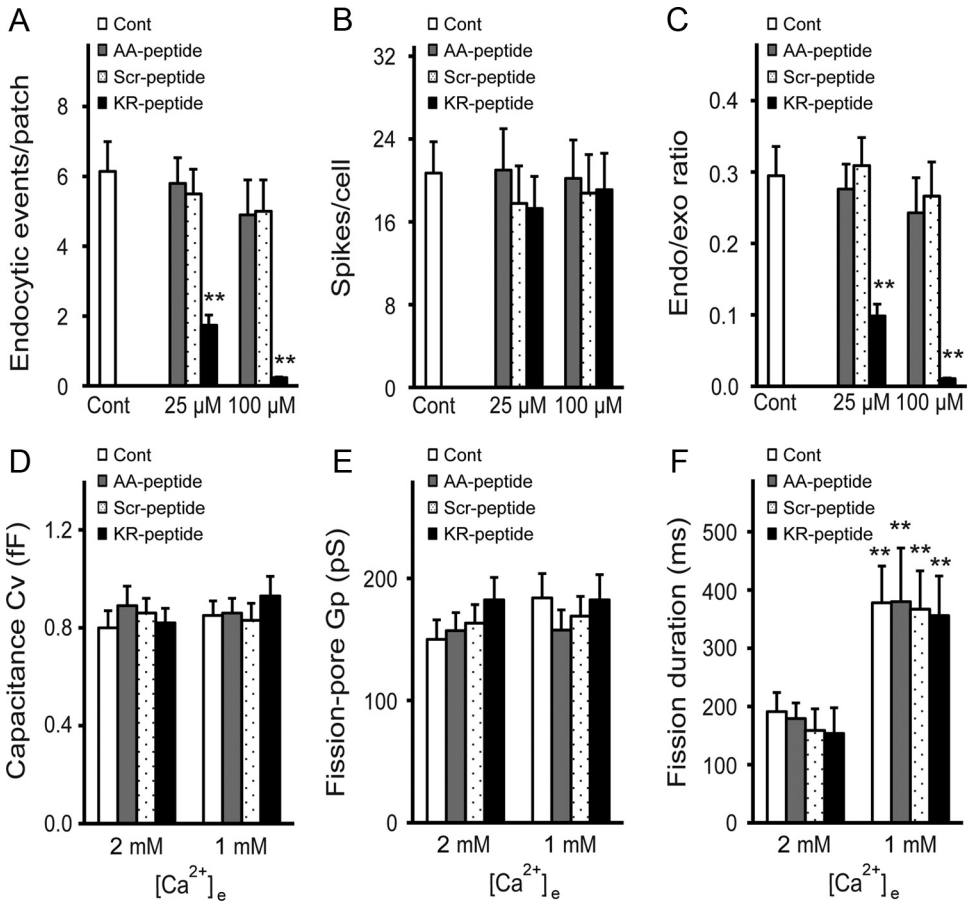

Figure 4. The fission-pore kinetics remain unaltered on disruption in Syt1–AP-2 interaction in double (cell-attached/whole-cell) patch configuration. KR-peptide, Scr-peptide, or AA-peptide was delivered into WT cells through the whole-cell patch pipette in double (cell-attached/whole-cell) patch configuration. ***A***, The number of endocytic events within 5 min of recordings at 2 mM $[Ca^{2+}]_e$ was reduced by KR-peptide (25 μM: $n = 129$ patches, $p < 0.01$; 100 μM: $n = 25$ patches, $p < 0.01$) but not by Scr-peptide (25 μM: $n = 97$ patches, $p > 0.05$; 100 μM: $n = 24$ patches, $p > 0.05$) or by AA-peptide (25 μM: $n = 133$ patches, $p > 0.05$; 100 μM: $n = 30$ patches, $p > 0.05$) compared to control ($n = 44$ patches). ***B***, Number of amperometric spikes indicating exocytotic events did not change in cells treated with KR-peptide (25 μM: $n = 27$ cells; 100 μM: $n = 17$ cells), Scr-peptide (25 μM: $n = 21$ cells; 100 μM: $n = 19$ cells), or AA-peptide (25 μM: $n = 16$ cells; 100 μM: $n = 14$ cells) compared to control cells ($n = 27$ cells) ($p > 0.05$). The experiments in ***A*** and ***B*** were performed in different cells from the same preparations. ***C***, Statistical analysis showed that the endocytosis/exocytosis ratio at 2 mM $[Ca^{2+}]_e$ was inhibited by KR-peptide ($p < 0.01$) but not Scr-peptide ($p > 0.05$) or AA-peptide ($p > 0.05$), indicating a role of Syt1–AP-2 interaction in regulating the endocytic capacity of CME. ***D***, Cv of the endocytic vesicles was not changed by 25 μM KR-peptide, Scr-peptide, or AA-peptide at both 1 (Control: $n = 52$ events; KR-peptide: $n = 47$ events; Scr-peptide: $n = 43$ events; AA-peptide: $n = 41$ events) ($p > 0.05$) and 2 mM $[Ca^{2+}]_e$ (Control: $n = 46$ events; KR-peptide: $n = 44$ events; Scr-peptide: $n = 40$ events; AA-peptide: $n = 53$ events) ($p > 0.05$). ***E***, The fission-pore Gp was comparable among these eight groups ($p > 0.05$). ***F***, Treatments with either KR-peptide, Scr-peptide, or AA-peptide produced no effects on the fission-pore duration at both 2 and 1 mM $[Ca^{2+}]_e$ ($p > 0.05$), indicating that disruption in Syt1–AP-2 interaction does not affect the Ca^{2+} dependence of fission-pore duration. $^{**}p < 0.01$.

that the numbers of endocytic events recorded in the two configurations were comparable (Figs. 1*F*, 2*A*, 3*B*, 4*A*). The number of endocytic events in the double-patch configuration could possibly be lowered due to a loss of some factors necessary for CME, when the cells are infused with intracellular solution in the whole-cell pipette. Consistent with this implication, a previous study has demonstrated that compensatory endocytosis, which occurs consistently in perforated patch configuration, shows rapid wash-out in the whole-cell configuration (Smith and Neher, 1997).

We have shown here that the dynamics of fission-pore closure in chromaffin cells is Ca^{2+} dependent, which is consistent with Ca^{2+}-dependent fission-pore kinetics in insulin-secreting INS-1 cells (MacDonald et al., 2005). In insulin-secreting cells, fission-pore kinetics exhibit two distinct kinetic components (Zhao et al., 2010). Further experiments will be necessary to determine whether this is also the case in chromaffin cells and whether the different kinetic components display different Ca^{2+} sensitivity.

The central finding of the present study is that the Ca^{2+} dependence of fission-pore kinetics requires Syt1. In the absence of Syt1, fission-pore dynamics is Ca^{2+} independent. The complete inhibition of endocytosis by the KR peptide at 100 μM concentration (Fig. 4*A*) indicates that endocytosis is mediated via an AP-2–Syt interaction. Similarly, a peptide derived from synaptotagmin 2 (Syt2) blocks CME in the calyx of Held where Syt2 is the predominant synaptotagmin isoform (Hosoi et al., 2009). Like Syt1 (Zhang et al., 1994), all synaptotagmin isoforms, including Syt4, bind AP-2 (Ullrich et al., 1994). In contrast to Syt1, the C2 domain of Syt4 does not display Ca^{2+} binding activity (Ullrich et al., 1994; Li et al., 1995; Dai et al., 2004). It is therefore possible that the endocytic events with Ca^{2+}-independent fission-pore dynamics in Syt1 KO cells are mediated by Syt4. Interestingly, a recent study showed that overexpression of Syt4 increased the endocytic fission-pore duration in PC12 cells (Zhang and Jackson, 2010), consistent with our result that at physiological $[Ca^{2+}]_e$, the fission-pore duration is increased in Syt1 KO cells (Fig. 3*G*,*H*).

It has been proposed that Syt4 may play a role in regulating neurotransmitter release (Moore-Dotson et al., 2010), fusion pore dynamics during exocytosis (Wang et al., 2001, 2003), and

granule maturation (Ahras et al., 2006) in PC12 cells, a chromaffin cell-derived cell line. However, in a recent immunocytochemical analysis confirming that Syt4 is also expressed in primary rat chromaffin cells, it was found that Syt4 was not present in dense core vesicles (Matsuoka et al., 2011). Our results suggest that, in the absence of Syt1, Syt4 may support endocytosis.

Although nuclear magnetic resonance studies have indicated that purified Syt1 has relatively low intrinsic Ca^{2+} affinity (Fernandez et al., 2001), recent evidence suggests that, when anchored to a membrane with physiological lipid composition, Syt1 displays Ca^{2+}-dependent enhancement in exocytosis even at submicromolar Ca^{2+} levels (Lee et al., 2010). Such Ca^{2+} levels are achievable in most nerve terminals following a single action potential or low-frequency stimulation, suggesting that Syt1 may serve as the Ca^{2+} sensor in endocytosis as well. Previous studies have noted that the rate of synaptic vesicle endocytosis is slower in Syt1 KO animals (Poskanzer et al., 2003, 2006; Nicholson-Tomishima and Ryan, 2004) but an elevation in $[Ca^{2+}]_e$ rescues the endocytic defect caused by a Syt1 mutant with low Ca^{2+} affinity (Poskanzer et al., 2006). However, due to the evidence that there exist multiple forms of endocytosis, such as CME, kiss-and-run, and bulk endocytosis in synapses (Wu et al., 2007), and that the contribution of each form of endocytosis in synaptic vesicle endocytosis varies markedly in different conditions such as when Ca^{2+} level is changed (Wu et al., 2009), the mechanism for the defect in synaptic vesicle endocytosis from Syt1 KO animals (Poskanzer et al., 2003, 2006; Nicholson-Tomishima and Ryan, 2004) remains uncertain. Our results identify that, in contrast to WT cells, the Ca^{2+} dependence of fission dynamics during CME is abolished in Syt1 KO cells (Fig. 3*H*), suggesting that Syt1 is a necessary component for the Ca^{2+} dependence of CME.

References

Ahras M, Otto GP, Tooze SA (2006) Synaptotagmin IV is necessary for the maturation of secretory granules in PC12 cells. J Cell Biol 173:241–251.

Albillos A, Dernick G, Horstmann H, Almers W, Alvarez de Toledo G, Lindau M (1997) The exocytotic event in chromaffin cells revealed by patch amperometry. Nature 389:509–512.

Beutner D, Voets T, Neher E, Moser T (2001) Calcium dependence of exocytosis and endocytosis at the cochlear inner hair cell afferent synapse. Neuron 29:681–690.

Breckenridge LJ, Almers W (1987) Currents through the fusion pore that forms during exocytosis of a secretory vesicle. Nature 328:814–817.

Ceccarelli B, Hurlbut WP (1980) Ca^{2+}-dependent recycling of synaptic vesicles at the frog neuromuscular junction. J Cell Biol 87:297–303.

Chapman ER (2008) How does synaptotagmin trigger neurotransmitter release? Annu Rev Biochem 77:615–641.

Chapman ER, Desai RC, Davis AF, Tornehl CK (1998) Delineation of the oligomerization, AP-2 binding, and synprint binding region of the C2B domain of synaptotagmin. J Biol Chem 273:32966–32972.

Chow RH, von Rüden L, Neher E (1992) Delay in vesicle fusion revealed by electrochemical monitoring of single secretory events in adrenal chromaffin cells. Nature 356:60–63.

Cousin MA, Robinson PJ (1998) Ba^{2+} does not support synaptic vesicle retrieval in rat cerebrocortical synaptosomes. Neurosci Lett 253:1–4.

Dai H, Shin OH, Machius M, Tomchick DR, Südhof TC, Rizo J (2004) Structural basis for the evolutionary inactivation of Ca^{2+} binding to synaptotagmin 4. Nat Struct Mol Biol 11:844–849.

Debus K, Lindau M (2000) Resolution of patch capacitance recordings and of fusion pore conductances in small vesicles. Biophys J 78:2983–2997.

Dernick G, Alvarez de Toledo G, Lindau M (2003) Exocytosis of single chromaffin granules in cell-free inside-out membrane patches. Nat Cell Biol 5:358–362.

Dernick G, Gong LW, Tabares L, Alvarez de Toledo G, Lindau M (2005) Patch amperometry: high-resolution measurements of single-vesicle fusion and release. Nat Methods 2:699–708.

Fernandez I, Araç D, Ubach J, Gerber SH, Shin O, Gao Y, Anderson RG, Südhof TC, Rizo J (2001) Three-dimensional structure of the synaptotagmin 1 C2B-domain: synaptotagmin 1 as a phospholipid binding machine. Neuron 32:1057–1069.

Gad H, Löw P, Zotova E, Brodin L, Shupliakov O (1998) Dissociation between Ca^{2+}-triggered synaptic vesicle exocytosis and clathrin-mediated endocytosis at a central synapse. Neuron 21:607–616.

Gong LW, Di Paolo G, Diaz E, Cestra G, Diaz ME, Lindau M, De Camilli P, Toomre D (2005) Phosphatidylinositol phosphate kinase type I gamma regulates dynamics of large dense-core vesicle fusion. Proc Natl Acad Sci U S A 102:5204–5209.

Gong LW, Hafez I, Alvarez de Toledo G, Lindau M (2003) Secretory vesicles membrane area is regulated in tandem with quantal size in chromaffin cells. J Neurosci 23:7917–7921.

Gong LW, de Toledo GA, Lindau M (2007) Exocytotic catecholamine release is not associated with cation flux through channels in the vesicle membrane but Na+ influx through the fusion pore. Nat Cell Biol 9:915–922.

Grass I, Thiel S, Höning S, Haucke V (2004) Recognition of a basic AP-2 binding motif within the C2B domain of synaptotagmin is dependent on multimerization. J Biol Chem 279:54872–54880.

Haucke V, De Camilli P (1999) AP-2 recruitment to synaptotagmin stimulated by tyrosine-based endocytic motifs. Science 285:1268–1271.

Hinrichsen L, Meyerholz A, Groos S, Ungewickell EJ (2006) Bending a membrane: how clathrin affects budding. Proc Natl Acad Sci U S A 103:8715–8720.

Hosoi N, Holt M, Sakaba T (2009) Calcium dependence of exo- and endocytotic coupling at a glutamatergic synapse. Neuron 63:216–229.

Kastning K, Kukhtina V, Kittler JT, Chen G, Pechstein A, Enders S, Lee SH, Sheng M, Yan Z, Haucke V (2007) Molecular determinants for the interaction between AMPA receptors and the clathrin adaptor complex AP-2. Proc Natl Acad Sci U S A 104:2991–2996.

Lee HK, Yang Y, Su Z, Hyeon C, Lee TS, Lee HW, Kweon DH, Shin YK, Yoon TY (2010) Dynamic Ca^{2+}-dependent stimulation of vesicle fusion by membrane-anchored synaptotagmin 1. Science 328:760–763.

Li C, Ullrich B, Zhang JZ, Anderson RG, Brose N, Südhof TC (1995) Ca(2+)-dependent and -independent activities of neural and non-neural synaptotagmins. Nature 375:594–599.

MacDonald PE, Eliasson L, Rorsman P (2005) Calcium increases endocytotic vesicle size and accelerates membrane fission in insulin-secreting INS-1 cells. J Cell Sci 118:5911–5920.

Marks B, McMahon HT (1998) Calcium triggers calcineurin-dependent synaptic vesicle recycling in mammalian nerve terminals. Curr Biol 8:740–749.

Marquèze B, Boudier JA, Mizuta M, Inagaki N, Seino S, Seagar M (1995) Cellular localization of synaptotagmin I, II, and III mRNAs in the central nervous system and pituitary and adrenal glands of the rat. J Neurosci 15:4906–4917.

Matsuoka H, Harada K, Nakamura J, Fukuda M, Inoue M (2011) Differential distribution of synaptotagmin-1, -4, -7, and -9 in rat adrenal chromaffin cells. Cell Tissue Res 344:41–50.

Moore-Dotson JM, Papke JB, Harkins AB (2010) Upregulation of synaptotagmin IV inhibits transmitter release in PC12 cells with targeted synaptotagmin I knockdown. BMC Neurosci 11:104.

Neher E, Marty A (1982) Discrete changes of cell membrane capacitance observed under conditions of enhanced secretion in bovine adrenal chromaffin cells. Proc Natl Acad Sci U S A 79:6712–6716.

Neher E, Sakaba T (2008) Multiple roles of calcium ions in the regulation of neurotransmitter release. Neuron 59:861–872.

Neves G, Gomis A, Lagnado L (2001) Calcium influx selects the fast mode of endocytosis in the synaptic terminal of retinal bipolar cells. Proc Natl Acad Sci U S A 98:15282–15287.

Nicholson-Tomishima K, Ryan TA (2004) Kinetic efficiency of endocytosis at mammalian CNS synapses requires synaptotagmin I. Proc Natl Acad Sci U S A 101:16648–16652.

Nossal R (2001) Energetics of clathrin basket assembly. Traffic 2:138–147.

Pang ZP, Südhof TC (2010) Cell biology of Ca2+-triggered exocytosis. Curr Opin Cell Biol 22:496–505.

Poskanzer KE, Marek KW, Sweeney ST, Davis GW (2003) Synaptotagmin I is necessary for compensatory synaptic vesicle endocytosis in vivo. Nature 426:559–563.

Poskanzer KE, Fetter RD, Davis GW (2006) Discrete residues in the c(2)b domain of synaptotagmin I independently specify endocytic rate and synaptic vesicle size. Neuron 50:49–62.

Ramaswami M, Krishnan KS, Kelly RB (1994) Intermediates in synaptic vesicle recycling revealed by optical imaging of Drosophila neuromuscular junctions. Neuron 13:363–375.

Rosenboom H, Lindau M (1994) Exo-endocytosis and closing of the fission pore during endocytosis in single pituitary nerve terminals internally perfused with high calcium concentrations. Proc Natl Acad Sci U S A 91: 5267–5271.

Sankaranarayanan S, Ryan TA (2001) Calcium accelerates endocytosis of vSNAREs at hippocampal synapses. Nat Neurosci 4:129–136.

Smith C, Neher E (1997) Multiple forms of endocytosis in bovine adrenal chromaffin cells. J Cell Biol 139:885–894.

Stevens CF (2003) Neurotransmitter release at central synapses. Neuron 40:381–388.

Ullrich B, Li C, Zhang JZ, McMahon H, Anderson RG, Geppert M, Südhof TC (1994) Functional properties of multiple synaptotagmins in brain. Neuron 13:1281–1291.

von Gersdorff H, Matthews G (1994) Inhibition of endocytosis by elevated internal calcium in a synaptic terminal. Nature 370:652–655.

Wang CT, Grishanin R, Earles CA, Chang PY, Martin TF, Chapman ER, Jackson MB (2001) Synaptotagmin modulation of fusion pore kinetics in regulated exocytosis of dense-core vesicles. Science 294:1111–1115.

Wang CT, Lu JC, Bai J, Chang PY, Martin TF, Chapman ER, Jackson MB (2003) Different domains of synaptotagmin control the choice between kiss-and-run and full fusion. Nature 424:943–947.

Wu LG, Ryan TA, Lagnado L (2007) Modes of vesicle retrieval at ribbon synapses, calyx-type synapses, and small central synapses. J Neurosci 27:11793–11802.

Wu W, Xu J, Wu XS, Wu LG (2005) Activity-dependent acceleration of endocytosis at a central synapse. J Neurosci 25:11676–11683.

Wu XS, McNeil BD, Xu J, Fan J, Xue L, Melicoff E, Adachi R, Bai L, Wu LG (2009) Ca(2+) and calmodulin initiate all forms of endocytosis during depolarization at a nerve terminal. Nat Neurosci 12:1003–1010.

Zhang JZ, Davletov BA, Südhof TC, Anderson RG (1994) Synaptotagmin I is a high affinity receptor for clathrin AP-2: implications for membrane recycling. Cell 78:751–760.

Zhang Z, Zhang Z, Jackson MB (2010) Synaptotagmin IV modulation of vesicle size and fusion pores in PC12 cells. Biophys J 98:968–978.

Zhao Y, Fang Q, Straub SG, Lindau M, Sharp GW (2010) Hormonal inhibition of endocytosis: novel roles for noradrenaline and G protein G(z). J Physiol 588:3499–3509.

Zucker RS, Regehr WG (2002) Short-term synaptic plasticity. Annu Rev Physiol 64:355–405.